Available online at www.sciencedirect.com
SCIENCE DIRECT®
Nuclear Instruments and Methods in Physics Research A 533 (2004) 305–321
NUCLEAR INSTRUMENTS & METHODS IN PHYSICS RESEARCH Section A
www.elsevier.com/locate/nima

Muon detection with a dual-readout calorimeter

N. Akchurin[a], K. Carrell[a], J. Hauptman[b], H. Kim[a], H.P. Paar[c], A. Penzo[d], R. Thomas[a], R. Wigmans[a,*]

[a]*Department of Physics, Texas Tech University, Box 41051, Lubbock, TX 79409-1051, USA*
[b]*Iowa State University, Ames, USA*
[c]*University of California at San Diego, La Jolla, USA*
[d]*INFN Trieste, Italy*

Received 10 May 2004; accepted 17 May 2004
Available online 23 July 2004

Abstract

Muon detection in a copper-based fiber calorimeter is studied by simultaneously measuring the scintillation light and the Cherenkov light generated in the detector. We report on the calorimeter response to muons ranging in energy from 20–300 GeV. Muons penetrate the full depth of a calorimeter and therefore can pass through the readout structure (in this case, bundled fibers, ferrules and PMT windows) generating signals not associated with the calorimeter proper. The availability of two physically separate readout signals makes it possible to recognize and eliminate these effects. A comparison of the scintillator and Cherenkov signals make it also possible to measure, for the first time, the separate contributions from ionization and radiation processes by muons in a massive medium.

Keywords: Sampling calorimetry; Bremsstrahlung; Cherenkov light; Optical fibers; Muons

1. Introduction

Muon detection is an important aspect of modern experiments in particle physics. Much of the new physics envisaged at future colliders is believed to be accessible through the muon channels. Accurate measurements of the muon momenta require first and foremost a high-precision magnetic spectrometer. However, the calorimeter system plays also an important role in identifying muons and measuring their properties, because

(1) The muons lose some fraction of their energy in the calorimeter by ionizing the absorber medium and, especially at high energies, by pair production and bremsstrahlung, with large event-to-event fluctuations. It is, therefore, important to measure this energy loss.

*Corresponding author. Tel.: +1-806-742-3779; fax: +1-806-742-1182.
E-mail address: wigmans@ttu.edu (R. Wigmans).

0168-9002/$ - see front matter © 2004 Elsevier B.V. All rights reserved.
doi:10.1016/j.nima.2004.05.134

(2) The calorimeter makes it possible to trace the muon on its way through the absorber, and thus link the track information obtained from measurements downstream and upstream from the calorimeter.
(3) The calorimeter is itself an important source of "fake" muons, produced by decaying pions and (most importantly) kaons generated in hadronic shower development in the absorber material. The calorimeter information may help in identifying such muons.

The DREAM calorimeter was developed as a dedicated detector for experiments at a future Linear e^+e^- Collider. It is equipped with both scintillating and undoped fibers. The signals from these two active media provide *complementary information* about the particles that generate these signals. The scintillating fibers produce light for every charged shower particle that crosses them. The amount of scintillation light is, in first approximation, proportional to the energy deposited by the shower particles in these fibers. On the other hand, the undoped fibers only produce (Cherenkov) light when they are traversed by charged particles traveling faster than the speed of light in the fiber material. Because of the dominant role of soft shower electrons, the amount of Cherenkov light generated in the undoped fibers is a measure of the energy carried by the electromagnetic (em) shower components. By measuring the signals from both types of fibers simultaneously, one can therefore determine what fraction of that energy was carried by the em shower component. We have shown that this method makes it possible to eliminate the dominant source of fluctuations in hadron showers [1].

In this paper, we study the properties of this calorimeter with respect to the detection of muons. Fiber calorimeters have specific problems when it comes to measuring particles which deposit only a fraction of their energy in the absorber volume and escape from the rear. Depending on the precise trajectory followed by the exiting particle, substantial additional contributions to the signals may be generated by interactions in the fibers and the photomultiplier tubes (PMTs) located in that area [2]. Obviously, this precludes a precise measurement of the energy loss of the muon on its way through the absorber.

In Sections 2 and 3, we describe the calorimeter, its calibration and the experimental setup in which it was tested. In Section 4, the experimental data and the methods used to analyze these data are presented. Experimental results are described and discussed in Section 5. We emphasize the information that can be derived from a comparison of the two types of signals generated by this calorimeter. This includes event-by-event information on the contribution of radiative and non-radiative energy loss mechanisms and a unique new way to determine the e/mip value, i.e. the absolute sampling fraction of em showers in this calorimeter. Also the readout problems mentioned above are alleviated substantially by the availability of two independent calorimeter signals. We have also measured the probability of muon production in hadron absorption in the setup in which the calorimeter was tested. Conclusions are summarized in Section 6.

2. The DREAM calorimeter

The measurements described in this paper were performed with a calorimeter that has become known by its acronym DREAM, for Dual-REAdout Module. The basic element of this detector (see Fig. 1) is an extruded copper rod, 2 m long and $4\times4\,mm^2$ in cross-section. This rod is hollow, the central cylinder has a diameter of 2.5 mm. In this hole are inserted seven optical fibers. Three of these are plastic scintillating fibers,[1] the other four fibers are undoped. The latter are intended for detecting Cherenkov light and, therefore, we will refer to these in the following as *Cherenkov fibers*. We used two different types of Cherenkov fibers. For the central region of the detector, high-purity quartz fibers[2] were used, while the peripheral regions of the detector were equipped with acrylic plastic fibers.[3] All fibers had an outer diameter of

[1]SCSF-81J produced by Kuraray Co. Ltd, Tokyo, Japan.
[2]Polymer-clad fused silica fibers, produced by Polymicro, Phoenix, USA.
[3]Raytela PJR-FB750, produced by Toray, Japan.

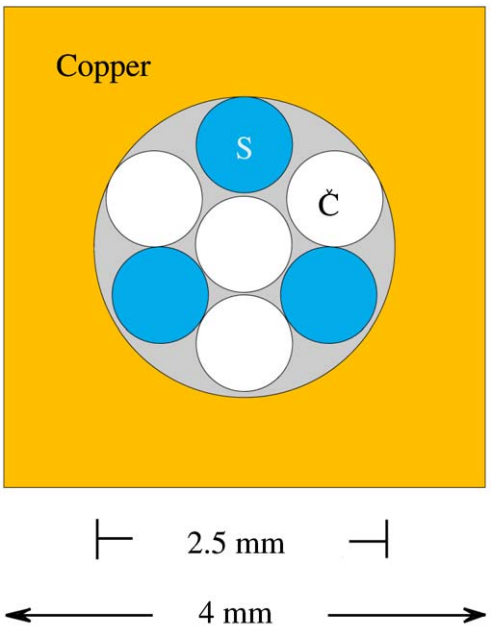

Fig. 1. The basic building block of the DREAM calorimeter is a $4 \times 4\,\mathrm{mm}^2$ extruded hollow copper rod of 2 meters length, with a 2.5 mm diameter central hole. Seven optical fibers (four Cherenkov and three scintillating fibers) with a diameter of 0.8 mm each are inserted in this hole, as shown.

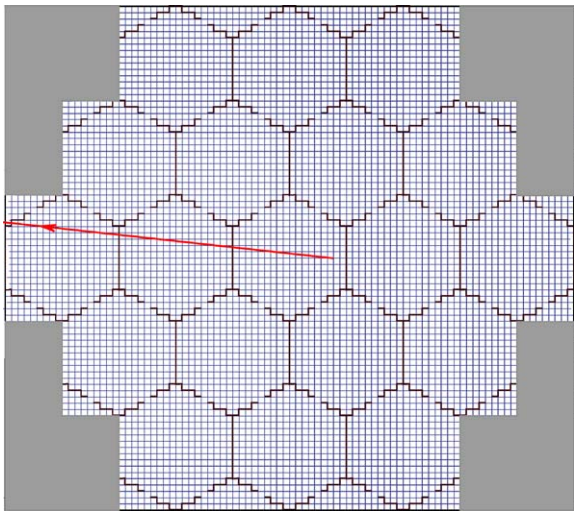

Fig. 2. Layout of the DREAM calorimeter. The detector consists of 19 hexagonal towers. A central tower is surrounded by two hexagonal rings, the Inner Ring (6 towers) and the Outer Ring (12 towers). The towers are not longitudinally segmented. The arrow indicates the (projection of the) trajectory of a muon traversing the calorimeter oriented in position D($6^\circ, 0.7^\circ$).

0.8 mm and a length of 2.50 m. The fiber pattern was the same for all rods, and is shown in Fig. 1.

The DREAM calorimeter consisted of 5580 such rods, 5130 of these were equipped with fibers. The empty rods were used as fillers, on the periphery of the detector. The instrumented volume thus had a length of 2.0 m, an effective radius of $\sqrt{5130 \times 0.16/\pi} = 16.2\,\mathrm{cm}$, and a mass of 1030 kg. The effective radiation length (X_0) of the calorimeter was 20.1 mm, the Moliére radius (ρ_M) was 20.4 mm and the nuclear interaction length (λ_{int}) 200 mm. The composition of the instrumented part of the calorimeter was as follows: 69.3% of the detector volume consisted of copper absorber, while the scintillating and Cherenkov fibers occupied 9.4% and 12.6%, respectively. Air accounted for the remaining 8.7%. Given the specific energy loss of a minimum-ionizing particle (mip) in copper (12.6 MeV/cm) and polystyrene (2.00 MeV/cm), the sampling fraction of the copper/scintillating-fiber structure for mip's was thus 2.1%.

The fibers were grouped to form 19 towers. Each tower consisted of 270 rods and had an approximately hexagonal shape (80 mm apex to apex). The layout is schematically shown in Fig. 2: A central tower, surrounded by two hexagonal rings, the Inner Ring (6 towers) and the Outer Ring (12 towers). The towers were longitudinally unsegmented.

The depth of the copper structure was 200 cm, or 99 X_0 ($10.0\lambda_{int}$). The fibers leaving the rear of this structure were separated into bunches: One bunch of scintillating fibers and one bunch of Cherenkov fibers for each tower, 38 bunches in total. In this way, the readout structure was established (see Fig. 3). Each bunch was coupled through a 2 mm air gap to a PMT.[4] In the case of the scintillating fibers, the window of the PMTs was covered with a yellow filter.[5] Since the dominant blue light from these fibers is attenuated by self-absorption (resulting from overlap of the

[4] Hamamatsu R-580, 10-stage, 1.5 in. diameter.
[5] Kodak, Wratten #3.

Fig. 3. Fiber bunches exiting from the rear face of the DREAM calorimeter. Each bunch was tightly squeezed by means of a thin metal collar with adjustable radius. In the following, we refer to these squeezed fiber bunches as "ferrules".

emission and absorption bands), this filter increased the light attenuation length of the fibers substantially. The Cherenkov fibers did not suffer from significant longitudinal non-uniformity, their light attenuation characteristics were adequate without filtering.

Fig. 3 shows a photograph of the fiber bunches exiting the downstream end of the calorimeter and the 38 PMTs used to detect their signals. In total, this detector contained about 90 km of optical fibers.

3. Experimental setup

3.1. The beam line

The measurements described in this paper were performed in the H4 beam line of the Super Proton Synchrotron at CERN. The DREAM detector was mounted on a platform that could move vertically and sideways with respect to the beam. Changing the angle of incidence of the beam particles with respect to the fibers in the horizontal plane (the ϕ angle) and the tilt angle (θ) was achieved with a crane.

Fig. 4. Schematic of the experimental setup in the beam line in which the DREAM detector was tested (see text for details).

The beam particle rates were typically several thousand per spill. The spills lasted 2.6 s and were repeated every 14.4 s. The widths of the collimators in the beam line were chosen so as to make the contribution of the momentum uncertainty of the beam particles negligible. The particle composition varied considerably, depending on the energy and the chosen collimator settings. In particular, low-energy hadron beams and high-energy electron beams contained considerable fractions of muons, the topic of the study presented in this paper.

We used several auxiliary detectors in the beam tests. These detectors served to obtain nearly pure samples of incident particles and to measure the impact point of these particles in the calorimeter event by event. Fig. 4 shows a schematic overview of the beam line, in which the positions of these auxiliary counters are indicated:

- Two small scintillation counters provided the signals that were used to trigger the data acquisition system. These trigger counters (TC) were 2.5 mm thick, and the area of overlap was $6 \times 6\,\mathrm{cm}^2$. A coincidence between the logic signals from these counters provided the trigger.
- The impact point of the beam particles was measured with a *fiber hodoscope* (HOD). This hodoscope consisted of 2 ribbons of scintillating fibers oriented in the horizontal or vertical direction, thus providing the y and x coordinates of the beam particles. The fibers were 500 μm in diameter, the position resolution was ~200 μm and the probability that a charged particle generated a signal above threshold was ~95% for each ribbon. Each fiber ribbon was read out by a position sensitive photomultiplier tube.[6] This hodoscope system was installed

[6]Hamamatsu R2486, equipped with 16×16 anode wires for position detection.

about 3 m upstream of the front face of the DREAM calorimeter. It made it possible to measure the coordinates of the impact point in the calorimeter with a precision of a fraction of 1 mm, depending on the beam energy.

- The *preshower detector* (PSD) consisted of a 5 mm thick ($1X_0$) lead absorber, followed by a scintillation counter whose pulse height was recorded. This simple device turned out to be extremely useful to eliminate beam contamination and was an important tool in obtaining event samples of high purity.
- Downstream of the calorimeter, behind an additional $8\lambda_{\text{int}}$ thick absorber, a $30 \times 30\,\text{cm}^2$ scintillation counter (MU) served to identify muons.

3.2. Data acquisition

The various detector signals were transported through RG-58 cables with (for timing purposes) appropriate lengths to the counting room. There, the signals to be digitized (i.e. all except those from the trigger counters and the fiber hodoscope) were fed into charge ADCs. Two types of ADCs were used for these tests. The signals from the central tower and the Inner Ring were read out by 11-bit LeCroy 2249 W ADCs, which have a total range of 0.5 nC (4 counts/pC). The signals from the 12 towers constituting the Outer Ring (see Fig. 2) were read out by 10-bit Lecroy 2249 ADCs, which have the same total range (2 counts/pC). All ADCs were operated at a gate width of 60 ns, the duration of the gate opened by the trigger signal was 120 ns, and the DREAM signals arrived ~30 ns after the trigger signal at the ADC.

The signals from the fiber hodoscope were fed into TDCs. In total, eight TDCs were used, four for the horizontal and vertical fiber ribbons, respectively. The time information could be converted into (x, y) coordinates of the point where the beam particle traversed the hodoscope.

The data acquisition system was based on CAMAC, interfaced via a VME bus to a Linux-based computer. At maximum, 8000 events could be recorded per 2.6 s SPS spill. The typical event size was ~150 bytes. All calorimeter signals, as well as the signals from all auxiliary detectors, could be monitored on-line.

3.3. Calibration of the detectors

Using the high voltage, the gain in the PMTs was set to generate ~2 pC/GeV in the central detector tower, ~4 pC/GeV in the Inner Ring and ~6 pC/GeV in the Outer Ring of the DREAM calorimeter. By choosing different gains, we effectively extended the limited dynamic range of our readout and thus increased its sensitivity to small energy deposits in the shower tails.

Each of the 19 towers was calibrated with 40 GeV electrons. The photomultiplier gains were chosen in such a way that the average signal for 40 GeV electrons entering in the center of a tower corresponded to about 300, 600 or 900 ADC counts above the pedestal value in that tower, depending on the chosen gain. On average, 92.5% of the scintillator light and 93.6% of the Cherenkov light was generated in that tower [3]. The signals observed in the exposed tower thus corresponded to an energy deposit of 37.0 GeV in the case of the scintillating fibers and of 37.4 GeV for the Cherenkov fibers. This, together with the precisely measured values of the average signals from the exposed tower, formed the basis for determining the calibration constants, i.e. the relationship between the measured number of ADC counts and the corresponding energy deposit. The stability of the calibration was checked four times during the test period by sending 40 GeV electrons into the center of each calorimeter tower and measuring the signal distribution. The mean values of these distributions were reproduced to better than 2% in these measurements, for all channels and for the entire test period of seven days.

4. Experimental data and methods

4.1. Experimental data

Events were triggered by coincident signals in the TC scintillation counters upstream of the calorimeter. Only events for which the (x, y)

coordinates of the beam particle in the fiber hodoscope were measured were retained for the analyses described in this paper. One of the purposes of the hodoscope information was to be able to limit the impact region of the beam particles. For example, for the analyses described in Sections 5.2 and 5.3, a circular region with a radius of 1.0 cm was selected.

The following data sets were used for these analyses:

(1) Negative pion data at 20, 40, 80, 100, 150, 200, 250 and 300 GeV, taken in the center of the DREAM calorimeter, with the detector oriented at $\phi = 2^\circ$ and $\theta = 0.7^\circ$ (position A).
(2) For the same detector orientation, high-statistics runs (1 million triggers or more) were available at four energies: 50, 100, 200 and 300 GeV. In these runs, a $0.1\lambda_{\text{int}}$ thick polyethylene target was placed in front of the calorimeter, but beam muons were of course not noticeably affected by this target.
(3) Negative pion data at 50, 100, 200 and 300 GeV, taken in the center of the calorimeter, with the detector oriented at the tilted position (B): $\phi = 3^\circ$, $\theta = 2^\circ$.
(4) Electron data at 20, 40, 80, 100, 150 and 200 GeV, both with the calorimeter oriented in position A$(2^\circ, 0.7^\circ)$ and in position B$(3^\circ, 2^\circ)$.
(5) Electron data at 40, 80, 100, 150 and 200 GeV, with the detector oriented in position D$(6^\circ, 0.7^\circ)$.

4.2. Event selection

Samples of muon events were selected by requiring a signal commensurate with that of a mip in the downstream MU counter (see Fig. 4). In order to make sure that the particle was beam associated, we also required a mip signal in the upstream preshower detector.

The only contaminating particles that survived these selection criteria were muons generated in hadronic shower development, i.e. from the decay of a pion or (more likely) kaon produced in the shower development. Such phenomena have been observed before [2], but were not expected to play a large role in our setup, given the relatively large distance between the calorimeter and the MU counter and the $8\lambda_{\text{int}}$ absorber between the calorimeter and the MU counter.

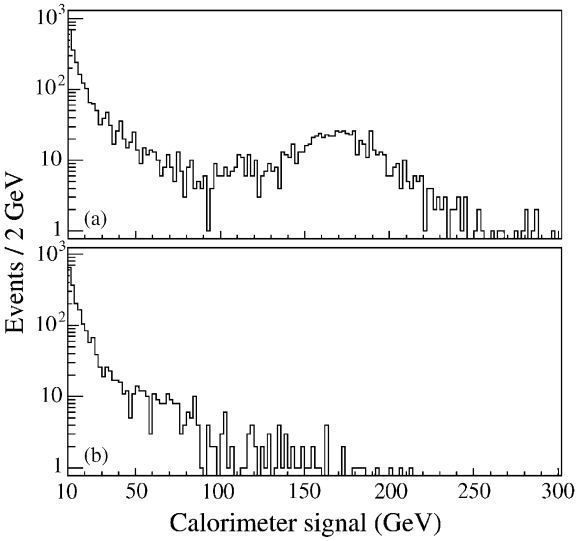

Fig. 5. The Landau tails of the (scintillator) signal distributions of muon samples obtained from the 200 GeV pion beam (a) and the 200 GeV electron beam (b). These distributions peak near 2 GeV, but only the spectral region above 10 GeV is shown in this figure. Both muon samples contained about 30,000 events.

We looked for such contaminating events by comparing the muon signal distributions from 200 GeV electron and 200 GeV pion runs. The contamination should only occur in the latter sample and would manifest itself as a high-energy bump superimposed on the Landau tail, since these events would essentially be hadron showers. Fig. 5 shows clear evidence for the effect. The muon spectrum obtained in the pion runs exhibits a significant bump around 170 GeV, where also the scintillator signal distribution from 200 GeV pions peaks.[7] No evidence for a bump near the beam energy is seen in the spectrum of muons from the electron beam.

The number of events in the pion bump (816) represents 0.22% of the number of pion events

[7]The calorimeter was calibrated with electrons. Since $e/h \approx 1.3$, the pion signals appear at a lower energy than the ones from electrons of the same energy.

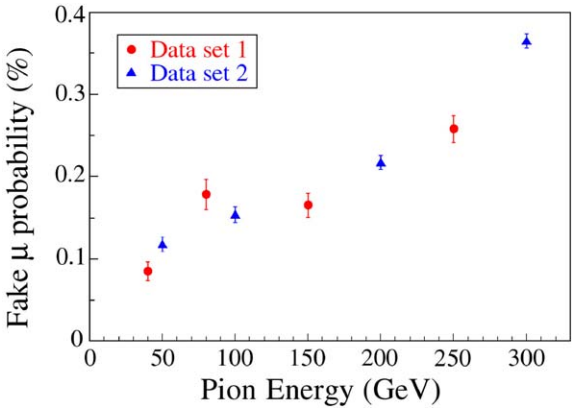

Fig. 6. The probability that a muon is generated in the development of a pion shower, travels through the absorber between the decay vertex and the MU counter and falls within the acceptance of this counter, as a function of the pion energy. Results are shown for runs taken under slightly different conditions (see Section 4.1).

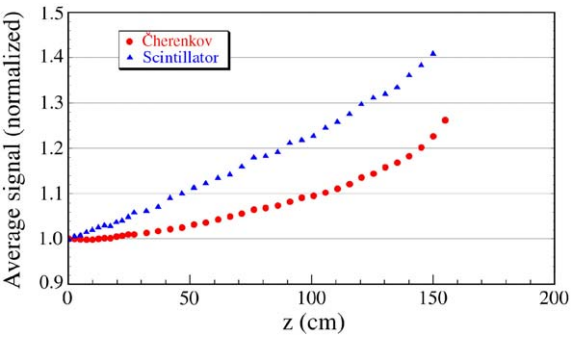

Fig. 7. The effects of light attenuation in the scintillating and the Cherenkov fibers. The average signals from 40 GeV electron showers are shown as a function of the (effective) depth at which the light production takes place. See text for details.

that passed all the cuts except the MU one. The probability that a muon is generated in the shower development of a 200 GeV pion, traverses the absorber material, and falls within the acceptance of the MU counter is thus 0.22%. This may be compared with the value of 2.3% measured by Acosta et al. for this energy [2]. We also measured the probability at other available energies, ranging from 40–300 GeV. The results are summarized in Fig. 6. The experimental data are approximately described by

$$P_{\text{fake}} = (1.1 \times 10^{-5})E_{\pi} \quad (1)$$

with the pion energy E_{π} expressed in units of GeV.

4.3. Corrections for light attenuation

Light attenuation in the optical fibers causes the calorimeter response to depend on the depth at which the light is produced. For em showers, which were used to calibrate the detector, the light is mostly produced at a depth of 20–30 cm inside the calorimeter. However, muons generate light along the full length of their trajectory. Since the light from muons is, on average, produced deeper inside the calorimeter, i.e. closer to the PMTs, it is less attenuated that of the em showers. Therefore, as described below, a weighting factor needs to be applied to the muon signals in order to correct for this effect.

The light attenuation characteristics were measured in great detail by rotating the detector at an angle of 24° in the horizontal plane and measuring the signals from 40 GeV electron showers as a function of the impact point along the full length of the fibers.[8] Fig. 7 shows the calorimeter response as a function of the depth at which the electrons deposited their energy. In the region close to the front face of the calorimeter ($z = 0$), where showers deposit most of their energy, the attenuation is well described by a single exponential function. However, deeper inside the calorimeter (i.e. at $z \gg 0$, close to the PMTs) this description is no longer valid. Since muons deposit their energy, on average, uniformly over the full depth of the calorimeter, we used the response averaged over the full depth as the basis for the correction. This average was larger than the response close to the front face, by 17% and 7% for the scintillator and Cherenkov channels, respectively. In order to eliminate the effects of light attenuation on the reconstructed muon energy deposit, the muon signals were thus weighted by factors 1/1.17 and 1/1.07 for these two channels. In this way, the muon signals are expressed in units of GeV, just like the calibration signals.

[8] These measurements are described in detail in Ref. [3].

5. Experimental results

5.1. DREAM effects on the muon signals

Unlike electrons, photons, hadrons and jets, which are in principle completely absorbed in the calorimeter, muons have the characteristic feature that they *traverse* the instrument and only lose a *fraction* of their energy while doing so. In the DREAM calorimeter, the muons exiting through the rear face subsequently traverse the readout section, a region of ~50 cm deep where the fibers are bunched, followed by the PMTs. This has specific consequences for the signals:

(1) The muons generate light in the fibers bunches, more so if they happen to traverse the tightly packed ferrule in front of the PMTs (see Fig. 3). The sampling fraction in this ferrule region is much higher than in the calorimeter itself and, moreover, the light is less attenuated. On the other hand, the Z of the fiber material is much lower than that of the copper absorber. Therefore, radiative energy losses, which dominate the muon energy loss at the high energies studied here, play much less of a role in this readout region.
(2) Muons traversing a PMT window generate Cherenkov light in this window. This affects the signals from the Cherenkov fibers much more than those from the scintillating fibers, since the scintillation photons are much more numerous than the Cherenkov ones. Therefore, the *relative* increase in the total light yield resulting from this effect is much larger for the Cherenkov channels than for the scintillator ones. We measured [3] that the light yield of the quartz fibers amounted to 8 photoelectrons per GeV deposited energy, while the clear plastic fibers generated 18 photoelectrons per GeV as a result of the Cherenkov effect. A mip traversing a glass window generates typically ~20 Cherenkov photons per mm [4]. Therefore, a muon traversing our PMTs (window thickness 2 mm) may easily contribute the equivalent of several GeV to the measured signal.

The first phenomenon leads to a general increase of the calorimeter signals, as well as a position dependence, since the increase depends on whether or not the track extrapolates to a ferrule. This is illustrated in Fig. 8. Fig. 8a shows the dependence of the average scintillator signal from 100 GeV muons on the impact point of the particles. This impact point was determined with the hodoscope. The beamspot was subdivided into 5 mm wide vertical slices for this study. The calorimeter was oriented in the "tilted" position, B(3°, 2°), for these measurements. The ferrule is clearly visible, muons entering the calorimeter in the region $0 < x < 5$ mm, travel through its center on their way out. These

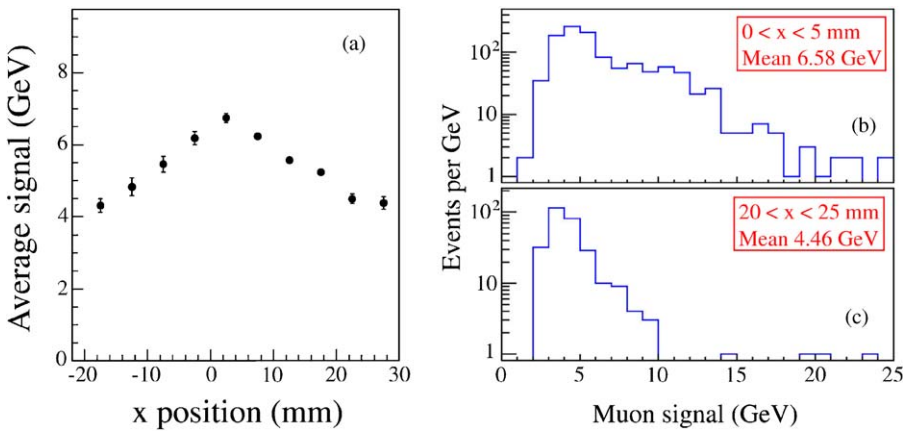

Fig. 8. Position dependence of the average scintillator signals from 100 GeV π^- (a) with the detector oriented in position B(3°, 2°), as well as typical muon spectra recorded at a maximum (b) and minimum (c).

muons produce a signal that, on average, is about 50% larger than those that miss it. The diameter of the ferrule, i.e. the bunch of 810 scintillating fibers from one hexagonal tower, is 23 mm, in good agreement with the width at half maximum of the "peak" observed in Fig. 8a.

Typical spectra for positions in which the average calorimeter signal is maximal or minimal are given in Figs. 8b and c, respectively. The difference between these spectra constitutes the contribution of the ferrule. This contribution manifests itself as a general shift to higher energies (the difference in peak position between the two spectra is about 1 GeV), as well as a much more pronounced high-energy tail. The latter effect is presumably the result of several particles traversing the ferrule simultaneously. This could happen, for example, when an incompletely contained bremsstrahlung shower leaves the calorimeter together with the primary muon.

The second phenomenon causes effects of a different order, at least for the Cherenkov signals. Fig. 9 shows the Cherenkov signal distributions for 100 GeV μ^- with the detector oriented in positions A$(2^\circ, 0.7^\circ)$ and B$(3^\circ, 2^\circ)$, respectively. In the latter case (Fig. 9b), the exiting muons exited the detector between PMTs. However, in position A$(2^\circ, 0.7^\circ)$, the untilted orientation (Fig. 9b), the muons traversed one of the PMTs that was used to read out the Cherenkov signals and generated a signal that, on average, was equivalent to ~10 GeV in this PMT alone.

Fig. 10a shows the position dependence of this effect. Thanks to the large beam spot, not all muons traversed the PMT when the detector was oriented in position A$(2^\circ, 0.7^\circ)$, for example those that entered the calorimeter at a position $x > 20$ mm. The spectrum of those muons (Fig. 10c) looked very similar to that of the muons measured with the detector oriented in position B$(3^\circ, 2^\circ)$ (Fig. 9b). On the other hand, the spectra of events in which the muons traverse a PMT on their way out exhibit a characteristic bump around 10 GeV. On average, the measured signal from these muons is *more than three times larger* than that of muons that miss the PMT, quite a difference from the 50% effect observed for the scintillator signals.

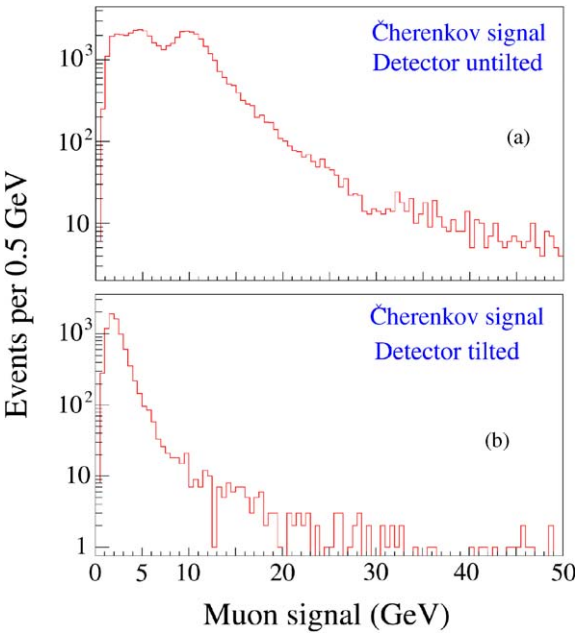

Fig. 9. Cherenkov signal distributions for 100 GeV μ^- with the calorimeter oriented in position A$(2^\circ, 0.7^\circ)$ (a) and B$(3^\circ, 2^\circ)$ (b), respectively.

A comparison of Figs. 10a and 8a shows not only this large difference in the magnitude of the effect, but it also illustrates that the effect observed for the Cherenkov signals is caused by the PMT and not by the ferrule that was responsible for the local increase in the scintillator signals. The "peak" in Fig. 10a is considerably broader than that in Fig. 8a, the width at half maximum is ~35 mm, much larger than the size of the ferrule, but compatible with the diameter of the PMT window (1.5″).

Interestingly, the spectra displayed in Figs. 9a and 10b have a more complicated structure than just the bump around 10 GeV. There seems to be a smaller second bump around 5 GeV. This bump is caused by particles that traverse the periphery of the PMT window, i.e. the part *not* covered by the quartz fiber ferrule. The quartz in this ferrule is itself also a prodigious source of Cherenkov photons, which is responsible for most of the additional signal contributions. This conclusion is confirmed by Fig. 11, which shows the impact point distributions for 100 GeV μ^- that caused signals of 2, 5 and 10 GeV in the Cherenkov

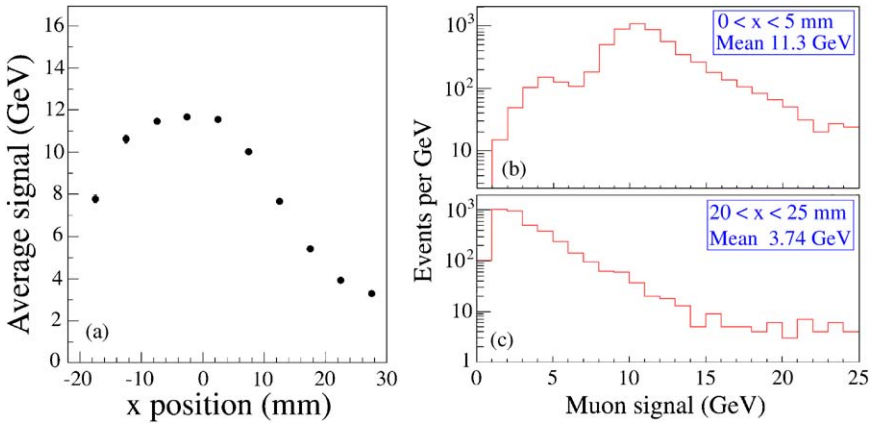

Fig. 10. The average Cherenkov signal from 100 GeV μ^- traversing the calorimeter oriented in position A(2°, 0.7°), as a function of the impact point of the particles (a). Cherenkov signal distributions for particles that traverse a PMT when exiting the calorimeter (b) and for particles that does not (c).

channel. In order to eliminate the effects of the intensity distribution within the beam spot, we have plotted the *fractions* of events that meet the energy selection criteria for each slice of the beam spot. These distributions are distinctly different. The particles causing the 5 GeV signals are strongly concentrated in a narrow region near the edge of the PMT. It is remarkable that our hodoscope can probe the position of the ferrule with respect to the PMT window through 2 m of copper.

The effects described above may give the impression that it is impossible to do meaningful measurements of the energy deposited by muons with the DREAM calorimeter. However, this is by no means true. The PMTs reading out the two signals from each tower are located at different positions. A muon exiting the calorimeter may traverse one or the other, *but not both*. Therefore, the availability of two independent signals makes it possible to determine which particles were affected by the phenomena described above and to what extent.

In Fig. 12, the Cherenkov signals from 100 GeV μ^- are plotted versus the scintillator signals for the same events, measured with the calorimeter in position A(2°, 0.7°). The size of the squares is an indication for the number of events contained in each bin. From this figure, it is clear which events were affected by the Cherenkov PMT. These

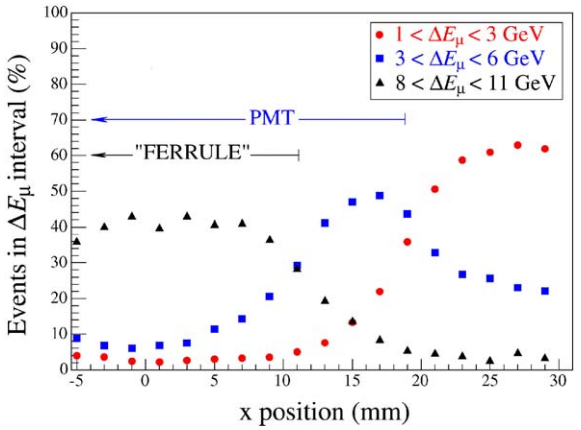

Fig. 11. (Normalized) impact point distributions of 100 GeV μ^- causing Cherenkov signals of 2, 5 and 10 GeV. The calorimeter is oriented in position A(2°, 0.7°).

events are concentrated in two areas centered around Cherenkov signals of about 5 and 10 GeV, respectively. Events in which the muons did not traverse a PMT are located in the shaded area.

One very simple way to estimate the energy lost by a given muon in the calorimeter is to use the *smaller* of the two signals for this purpose. Since at least one of the two signals is unaffected by the phenomena described in this subsection, selecting the smaller of the two signals should greatly reduce the effects of the readout on the measured energy loss. We tested this hypothesis with a sample of

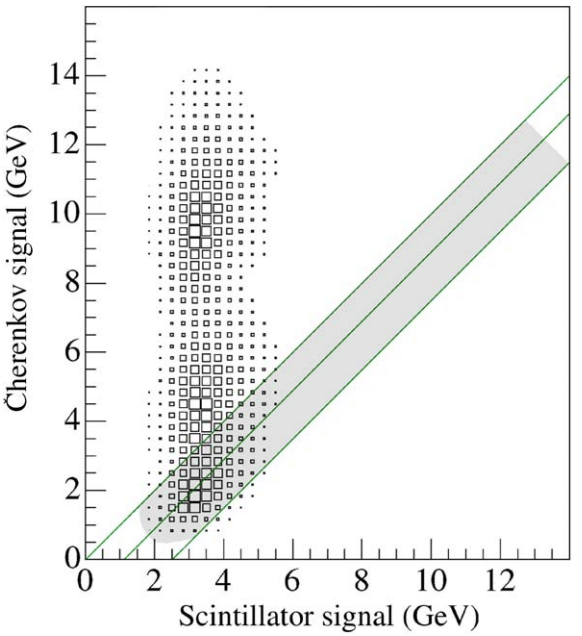

Fig. 12. The Cherenkov signals for 200 GeV μ^- versus those generated by the scintillating fibers in the DREAM calorimeter. The calorimeter is oriented in position A($2^\circ, 0.7^\circ$). The size of the squares is an indication for the number of events contained in each bin of this plot.

100 GeV μ^- events, containing equal numbers of events from the runs in position A($2^\circ, 0.7^\circ$) and position B($3^\circ, 2^\circ$). The sample contained in total 14384 events, chosen at random.

Figs. 13a and b show the (scintillator and Cherenkov) signal distributions for the 8829 events for which the Cherenkov signal was smaller than the scintillator signal. For comparison, we show in Figs. 13c and d the distributions of the (scintillator and Cherenkov) signals measured for 100 GeV μ^- with the detector oriented in position D($6^\circ, 0.7^\circ$). In the latter case, the exiting muons *physically missed* the entire readout region, which therefore did not contribute at all to the signals. Apart from an overall scale factor, which reflects the difference in path length through the detector (including the fibers sticking out in the rear), the latter distributions are remarkably similar to the ones resulting from our simple selection criterion, proving its effectiveness in eliminating the anomalous effects of the readout on the measured energy loss. The same conclusion could be drawn from the 5555 events in which the scintillator signal was the smaller of the two signals.

The availability of two independent signals thus provides a simple and effective way to measure the energy loss of muons in this calorimeter, since it eliminates the uncertainties introduced by the readout system. However, for a detailed comparison of the information provided by the two different types of signals, we turn to the data taken with the calorimeter in position D($6^\circ, 0.7^\circ$), where contributions of the readout system to the signals did not play any role whatsoever (data set 5, see Section 4.1).

5.2. The 6° data

When the calorimeter was oriented in position D($6^\circ, 0.7^\circ$), the impact point of the particles was chosen such that the center-of-gravity of 40 GeV electron showers projected onto the center of the calorimeter. Since this center-of-gravity was located at a depth $z \approx 25$ cm inside the calorimeter, the impact point was thus displaced by $25 \sin 6^\circ = 2.6$ cm with respect to the center of the calorimeter. The projection of the trajectory of muons traversing the calorimeter onto its front face is shown in Fig. 2. This projection has an average length of 20.4 cm. Therefore, the muons left the calorimeter sideways at a depth of $20.4/\sin 6^\circ = 195$ cm and thus did *not* traverse the readout region that may disturb the signals as discussed in the previous subsection.

At the high energies considered here, muons are by no means minimum ionizing particles (mips). The energy loss per unit length may be considerably larger than the mip value, due to phenomena such as δ-ray emission (relativistic rise), bremsstrahlung, e^+e^- pair production and, at very high energies, nuclear reactions. The contribution of these effects to the total energy loss is strongly dependent on the muon energy and on the Z value of the material [5]. The *critical energy* for muons, i.e. the energy at which the average energy loss per unit material is equal for the bremsstrahlung and ionization components, is larger than that for electrons by a factor of the order of $(m_\mu/m_e)^2 \approx 40,000$. Using the expression given by the Particle Data Group, $E_{\mu c} =$

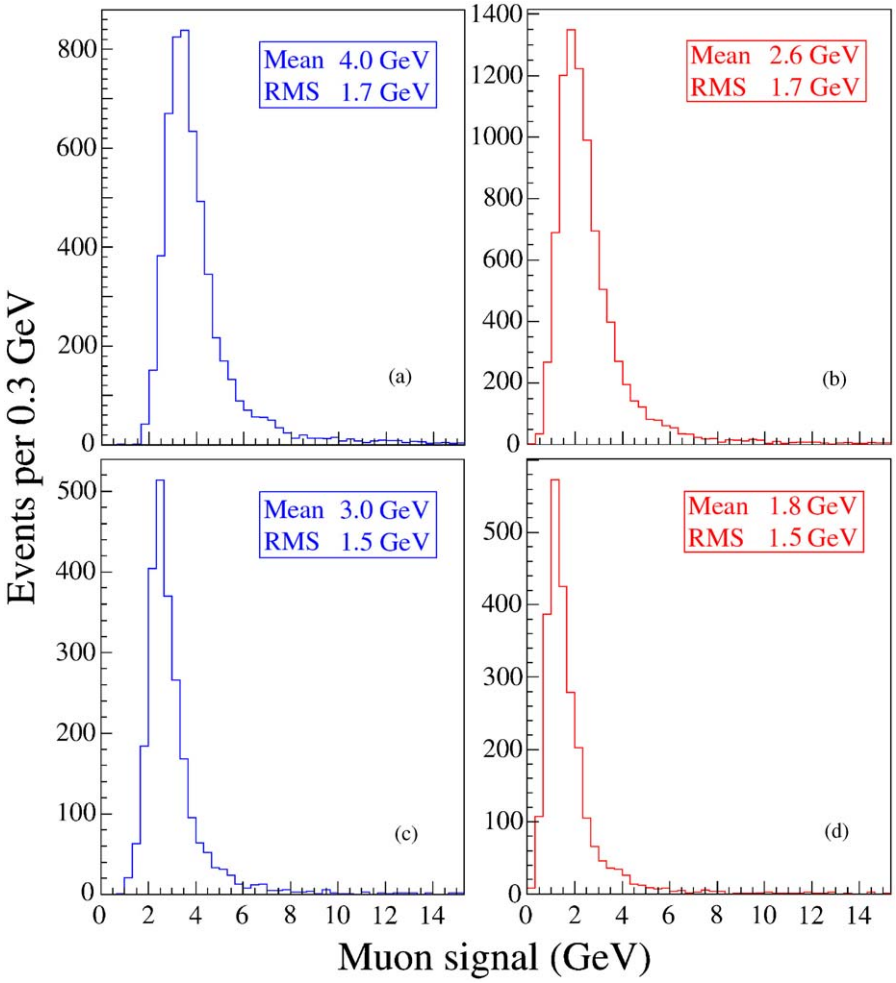

Fig. 13. Distribution of the measured energy loss of 100 GeV muons on the basis of the scintillator signal (a) or the Cherenkov signal (b), with the calorimeter oriented in either position A($2^\circ, 0.7^\circ$) or position B($3^\circ, 2^\circ$). For reference purposes, the signal distributions from the scintillating fibers (c) and the Cherenkov fibers (d), measured in position D($6^\circ, 0.7^\circ$) where the muons did not traverse the readout region, are shown as well.

$5700\,\mathrm{GeV}/(Z+1.47)^{0.879}$ [6], one expects the energy at which radiation and ionization processes contribute equally to the energy loss of the muons in copper ($Z=29$) to be $\sim$300 GeV.

The scintillator signal distributions for muons at 40, 100 and 200 GeV are shown in Fig. 14. A comparison between the high-energy tails of these distributions illustrates the increased importance of radiative energy losses as the muon energy increases. This is also illustrated in Fig. 15, where the average energy loss of the muons, measured by the scintillating fibers, is given as a function of the muon energy. This average, expressed in GeVs as determined on the basis of the electron calibration, increases gradually from 2.1 at 20 to 3.5 at 200 GeV. The question, to be answered in the next subsection, is to what extent this energy calibration is also valid for the energy deposited by muons.

Fig. 16 shines some very interesting light on this issue. In this figure, the spectra for 200 GeV muons traversing the DREAM calorimeter at 6°

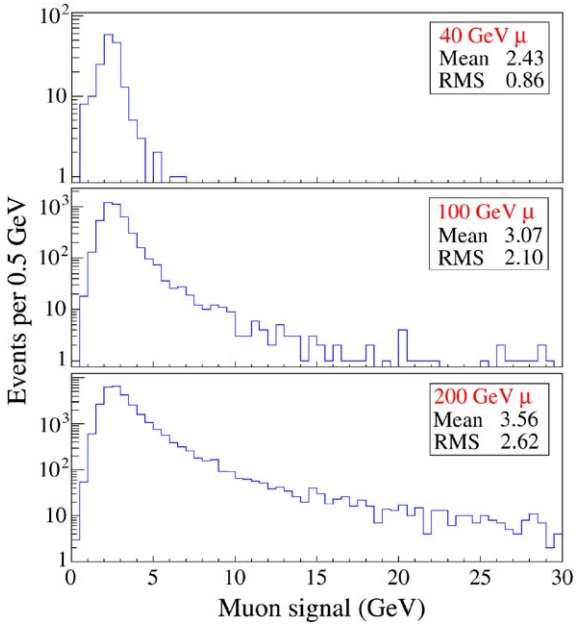

Fig. 14. Signal distributions for 40, 100 and 200 GeV muons, measured with the scintillating fibers in the DREAM calorimeter.

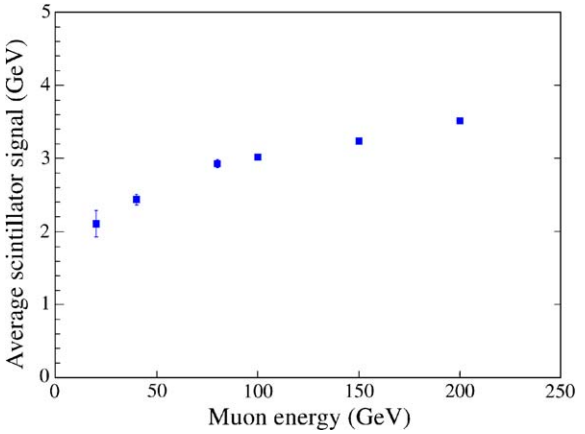

Fig. 15. Average signal from muons traversing the DREAM calorimeter, as a function of the muon energy. The detector was oriented in position D(6°, 0.7°).

are compared for the scintillator and the Cherenkov channels. The radiative tails of both spectra seem identical, but the energy at which the spectra reach their maximum is very different for both spectra. Fits with a Landau distribution yielded the following values for the most probable value of

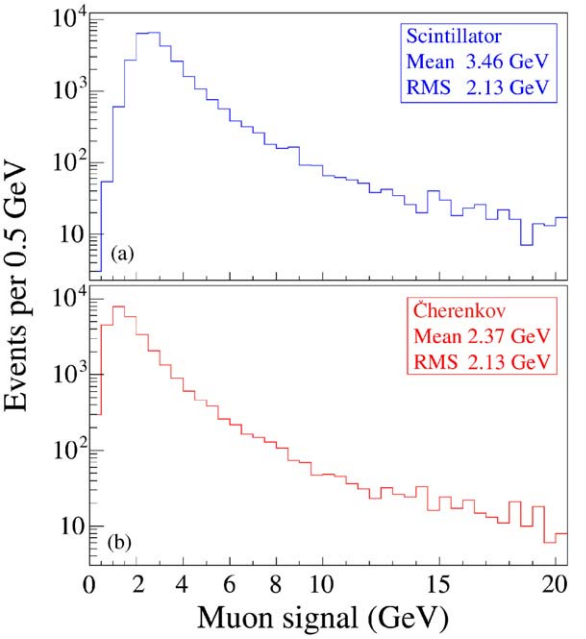

Fig. 16. Signal distributions for 200 GeV muons, measured with the scintillating and the Cherenkov fibers in the DREAM calorimeter.

the calorimeter signal: 2.417 ± 0.005 GeV and 1.236 ± 0.004 GeV for the scintillator and Cherenkov signals, respectively. A difference of a factor of two! At lower energies, the relative difference was even larger, but *the absolute difference between the two values remained the same*, as illustrated by Table 1, which summarizes these results. The same data are also shown in Fig. 17.

The explanation of this remarkable phenomenon is as follows. Muons traversing the calorimeter lose energy by ionization and by radiation. In the latter process, the particles radiate photons which, if sufficiently energetic, develop electromagnetic showers. Since the calorimeter was calibrated with em showers, the signal distribution for this energy loss component should be *exactly the same* for the two readout media. Where they differ is in the ionization component. If we ignore the effects of multiple scattering, the muon travels at an angle of 6 degrees with the fibers. Particles that generate a signal in the Cherenkov fibers need to traverse these fibers at an angle that falls within a trapping cone around an axis that is oriented at 46° (the Cherenkov

Table 1
The most probable values, as determined by Landau fits, of the scintillator and Cherenkov signals from muons traversing the DREAM calorimeter oriented in position D(6°, 0.7°). All values are expressed in units of GeV, as determined by the electron calibration of the calorimeter

Muon energy	Scintillator signal	Cherenkov signal	Difference
40	2.133 ± 0.038	0.962 ± 0.022	1.171 ± 0.044
80	2.210 ± 0.020	1.058 ± 0.012	1.152 ± 0.023
100	2.241 ± 0.009	1.088 ± 0.007	1.153 ± 0.011
150	2.301 ± 0.004	1.145 ± 0.003	1.156 ± 0.005
200	2.417 ± 0.005	1.236 ± 0.004	1.181 ± 0.007

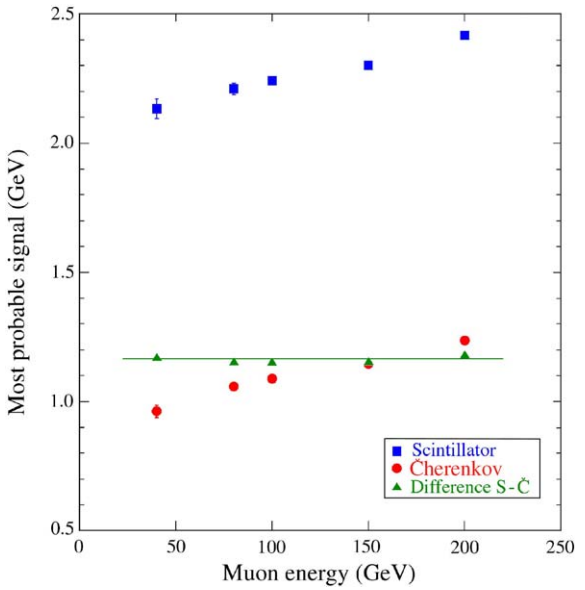

Fig. 17. Most probable signal from muons traversing the DREAM calorimeter, as a function of the muon energy. The detector was oriented in position D(6°, 0.7°). Results from fits to a Landau distribution are given separately for the scintillating and the Cherenkov fibers. Also shown is the *difference* between the most probable signal values from both media.

angle) with the fiber axis. This trapping cone is determined by the numerical aperture of the fibers. It has an opening angle of 19° for the quartz fibers and of 30° for the plastic ones [4]. Since the muons fall outside these trapping cones, we conclude that the non-radiative energy losses of the muons traversing the calorimeter, in first approximation, do *not lead to any signal* in the Cherenkov fibers. The signals from the scintillating fibers are not subject to these directionality considerations. Therefore, the constant difference observed between the most probable signals from the two active media of this calorimeter is a measure for the energy lost by the muons in the form of ionization of the traversed material. This energy loss is constant, i.e. independent of the muon energy. The radiative losses gradually increase with the muon energy, as illustrated in Fig. 17.

One may wonder to what extent a Landau fit is a reasonable description of the muon energy loss, especially given this exceptional characteristic of the Cherenkov fibers. Therefore, we also compared the *average* signals from the two types of fibers. The results, listed in Table 2 and shown in Fig. 18, exhibit exactly the same characteristic as observed for the most probable signal values. The difference between the average signals from the scintillating fibers and the Cherenkov fibers is independent of the muon energy, and it is within experimental errors equal to the difference between the most probable values for the signals from these two media: 1.169 GeV (average) vs 1.163 GeV (most probable).

To our knowledge, the DREAM calorimeter is the first instrument ever to demonstrate and measure the difference between the radiative and ionization losses of muons traversing material.

5.3. The e/mip ratio

In this subsection we discuss the absolute value of the calorimeter signals. We can say something about that by determining the so-called e/mip ratio. This ratio relates the signals from em

Table 2
The average scintillator and Cherenkov signals from muons traversing the DREAM calorimeter oriented in position D(6°, 0.7°). All values are expressed in units of GeV, as determined by the electron calibration of the calorimeter

Muon energy	Scintillator signal	Cherenkov signal	Difference
40	2.432 ± 0.066	1.357 ± 0.064	1.075 ± 0.092
80	2.923 ± 0.051	1.762 ± 0.055	1.161 ± 0.075
100	3.016 ± 0.026	1.870 ± 0.030	1.146 ± 0.040
150	3.235 ± 0.011	2.069 ± 0.011	1.166 ± 0.016
200	3.511 ± 0.014	2.326 ± 0.014	1.185 ± 0.020

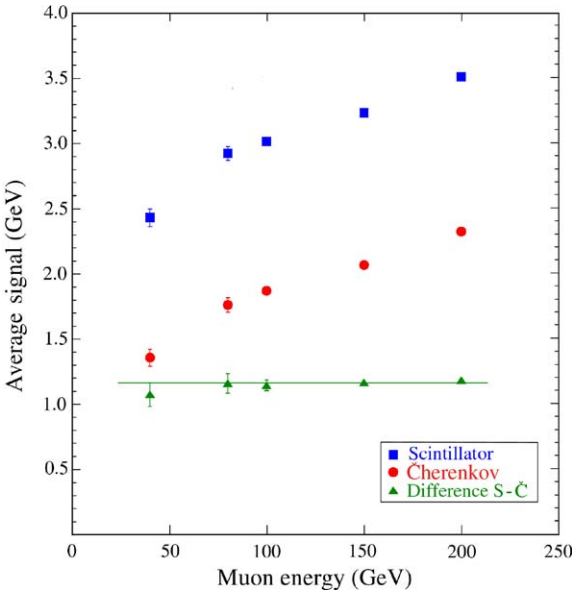

Fig. 18. Average signal from muons traversing the DREAM calorimeter, as a function of the muon energy. The detector was oriented in position D(6°, 0.7°). Results are given separately for the scintillating and the Cherenkov fibers. Also shown is the *difference* between the average signal values from both media.

showers to those of minimum ionizing particles depositing the same amount of energy in the calorimeter. Since the sampling fraction and the amount of energy lost in the detector by a mip are precisely known from the composition of the calorimeter and from the specific ionization losses ($\langle dE/dx \rangle$) in the various materials composing it, a measurement of the e/mip value is equivalent to an absolute measurement of the sampling fraction for an em shower.

Our calorimeter consists of 69.3% copper, 9.4% plastic scintillator, 8.0% clear plastic, 4.6% quartz and 8.7% air. It is 200 cm long. A mip thus deposits, on average, 1834 MeV in this structure, out of which 37.6 MeV is deposited in the plastic scintillator. The sampling fraction of a mip in the plastic scintillator is thus 2.05%. Since the total track length of the muons in the D(6°, 0.7°) geometry is 195 cm, a mip loses on average 1788 MeV in the calorimeter in these measurements. According to Tables 1 and 2, a 40 GeV muon loses on average 2.432 GeV and the most probable value of the energy loss amounts to 2.133 GeV. If we interpret the latter number as the mip value (which is certainly incorrect for thin absorbers because of the stochastic nature of the energy loss process), we find an e/mip value of $1788/2133 = 0.838 \pm 0.015$, where the error is statistical only. The corresponding sampling fraction for em showers in the copper/plastic-scintillator structure is $0.838 \times 2.05\% = 1.72\%$, and this number may be compared to Monte Carlo simulations.

Fig. 19 shows the results of EGS4 calculations, together with experimental e/mip values from this and other experiments. The agreement with the results of these calculations seems to be good. However, it should be pointed out that the precise value of the e/mip ratio depends on the sampling frequency of the detector [10]. The calculations of which the results are depicted in Fig. 19 concern a "sandwich" geometry, in which 1 X_0 thick absorber plates are alternated with 2.5 mm thick slabs of plastic scintillator. The shower sampling tends to be more efficient (i.e. a larger e/mip ratio) in fiber calorimeters.

The problem with the above analysis, which follows the examples set by HELIOS [7], ZEUS [8] and SPACAL [9], is that a 40 GeV muon is not a mip. As a matter of fact, mip's are hypothetical particles, they do not exist. Since a muon is the closest thing to a mip that nature provides us with, we use the muon data for doing this analysis.

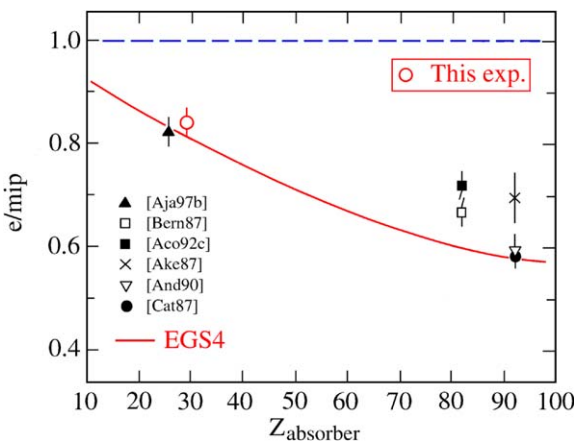

Fig. 19. The e/mip ratio of the Cu/scintillator structure, together with other published results and the prediction of EGS4 for metal/scintillator calorimeters.

However, it is clear that the average signal from 40 GeV muons contains non-mip contributions. It is not clear how to unfold these contributions from first principles. Also, the fact that the most probable signal value is a function of energy (Fig. 17) is at odds with the assumption that this value is representative for a mip.

There is clearly no unambiguous way to determine the e/mip value experimentally from muon measurements at different energies. In this context, our observation of a constant difference between the signals from the scintillating fibers and the Cherenkov fibers in the DREAM calorimeter may provide a unique alternative. As we saw in Section 5.2, this difference is due to the ionization processes in the energy loss, which do contribute to the scintillator signals, but not to the Cherenkov signals. Based on the calibration with em showers, we found that these ionization losses amounted to 1.166 ± 0.003 GeV, whereas a mip would lose 1.788 GeV along the same path. The ratio of these two numbers, which we will call $(S - C)$/mip, is a very precisely and unambiguously measurable alternative for the e/mip value. It measures essentially the same thing as the e/mip ratio, namely to what extent does an em shower resemble a collection of mip when it comes to the signal from a sampling calorimeter? However, whereas the experimental value of $(S - C)$/mip can be very precisely measured (0.652 ± 0.002 in our case), its relationship with e/mip will require some detailed Monte Carlo simulations which are beyond the scope of the present study.

6. Conclusions

We have investigated the signals from high-energy muons in a novel type of sampling calorimeter, equipped with two independent active media, scintillating fibers (for the measurement of the energy deposit dE/dx) and fibers measuring the production of Cherenkov light. This calorimeter was primarily designed for the detection of hadrons and jets. Unlike showering particles, muons are not absorbed in this detector. They exit from the rear, where the readout of the detector is located. We found that light produced in the fibers and the PMT windows behind the detector may significantly affect the muon signals. This is particularly true for the Cherenkov signals, which may be quadrupled by this effect. However, thanks to the fact that at least one of the two signals was *not* affected by this phenomenon, it was still possible to measure the energy loss accurately for each and every muon that traversed the calorimeter. This is a major and important advantage over fiber calorimeters that would only produce one signal.

When the muons were sent through the calorimeter avoiding the readout structure, an interesting phenomenon was observed. The signals measured with the scintillating fibers were systematically larger than those from the Cherenkov fibers. The difference was independent of the muon energy (for muons in the range from 40–200 GeV) and it was the same for the average and the most probable signals. The reason for this difference is the fact that the ionization losses did not lead to a signal in the Cherenkov fibers, since the Cherenkov light did not fall within the trapping cone. The Cherenkov fibers only measured the radiative (bremsstrahlung) losses and, therefore, a comparison of the signals from the two media made it possible to separate the contributions of ionization and radiative energy losses by the muons.

The e/mip value of the copper/scintillator calorimeter structure was measured to be 0.838 ± 0.015, in good agreement with expectations on the basis of EGS4 simulations. The probability of muon production in the hadronic absorption process was measured to be $1.1 \times 10^{-5} E_\pi$ (GeV), in the setup in which the calorimeter was tested.

Acknowledgements

We gratefully acknowledge the contributions of Tracy McAskill, Vladimir Nagaslaev, Alan Sill, Veronica Stelmakh, Yunyong Wang, Erika Washington and Kim Zinsmeyer to the construction of the DREAM detector. We thank CERN for making particle beams of excellent quality available. Our beam tests would not have been possible

without the help we received from Claude Ferrari and Maurice Haguenauer. We thank K. Kuroda for loaning us the fiber hodoscopes, and A. Gorin and I. Manouilov for their assistance with the data acquisition system. This study was carried out with financial support of the United States Department of Energy, under contract DE-FG02-95ER40938, and the Advanced Research Program of the State of Texas.

References

[1] N. Akchurin, et al., Hadron and jet detection with a dual-readout calorimeter, Nucl. Instr. and Meth., in press; http://highenergy.phys.ttu.edu/dream/.
[2] D. Acosta, et al., Nucl. Instr. and Meth. A 309 (1991) 143.
[3] N. Akchurin et al., Electron detection with a dual-readout calorimeter, Nucl. Instr. and Meth., submitted for publication; http://highenergy.phys.ttu.edu/dream/.
[4] N. Akchurin, R. Wigmans, Rev. Sci. Instr. 74 (2003) 2955.
[5] W. Lohmann, R. Kopp, R. Voss, Energy loss of muons in the energy range 1 GeVs to 10 TeVs CERN, Yellow Report 85-03, 1985.
[6] D.E. Groom, et al., Eur. Phys. J. C15 (2000) 1.
[7] T. Åkesson, et al., Nucl. Instr. and Meth. A 262 (1987) 243.
[8] E. Bernardi, et al., Nucl. Instr. and Meth. A 262 (1987) 229.
[9] D. Acosta, et al., Nucl. Instr. and Meth. A 320 (1992) 128.
[10] R. Wigmans, Calorimetry—energy measurement in particle physics, in: International Series of Monographs on Physics, vol. 107, Oxford University Press, Oxford, 2000.